2018

Artificial Neural Networks for Fast Rooftop Unit Fault Impact Modeling and Simulation

Andrew L. Hjortland
Purdue University, United States of America, andrew.hjortland@gmail.com

James E. Braun
Purdue University - Main Campus, jbraun@purdue.edu

Artificial Neural Networks for Fast Rooftop Unit Fault Impact Modeling and Simulation

Andrew L. HJORTLAND*, James E. BRAUN

Purdue University
Department of Mechanical Engineering,
West Lafayette, IN, USA
Andrew.Hjortland@gmail.com
* Corresponding Author

ABSTRACT

Like any electromechanical system, direct-expansion (DX) air conditioners and heat pumps often develop faults over time that contribute to reduced operating efficiency, more frequent comfort violations, or even premature failure. Automated fault detection and diagnosis (AFDD) methods have been developed for these systems and much experimental effort has been undertaken for their evaluation. In order to reduce development costs required for AFDD technologies, additional research related to modeling DX equipment subject to faults has been undertaken. Investigation of AFDD methods in a virtual environment typically requires relatively detailed equipment models based in some part on thermodynamic principles. Because of these embedded constraints, simulation of faulty equipment operating performance can be time consuming and computationally intensive. In this work, meta-models based on previously developed greybox fault impact models for DX equipment have been developed using artificial neural networks. After tuning these neural network meta-models for different equipment, AFDD performance and fault impacts were simulated using a simple building load model. Significant computational speedups (>3000 times faster) were realized over the original greybox equipment models without loss of significant accuracy. Ultimately through careful meta-model training, it is believed that using neural networks to approximate detailed, computationally-intensive equipment or building models may be useful in applications that require frequent model evaluations.

1. INTRODUCTION

A commonly held belief among engineers is that to truly understand the underlying phenomena of a physical system, an engineer needs to formulate a model of such a system based on the known principles of nature governing the processes involved. As the complexity of a system grows, it's generally accepted that the model required for estimating the physics of the system must also be extended to account for additional variables that affect its performance. Of course, adding complexity to models can often require ever more increasing engineering and computational effort (with sometimes diminishing returns). Because of this tradeoff, every engineer must determine the balance between complexity and effort that is suited for each project at hand.

One example of a relatively complex approach for modeling the performance impacts of common faults affecting unitary air conditioning equipment has been described by Cheung and Braun (2013a, 2013b). In this work, Cheung and Braun formulated detailed models of common air conditioning equipment components using engineering principles. Components modeled in this work included compressors, air-cooled condensers, expansion devices, cooling coils, and refrigerant piping. To tune difficult or unmeasurable parameters used in component models, Cheung and Braun used inverse modeling methods applied to experimental data collected from actual systems. Finally, component models were integrated into system models which imposed additional constraints to maintain conservation of mass and energy throughout the closed system.

In comparison with other methodologies developed for estimating fault impacts of DX air conditioning equipment, the methodology presented by Cheung and Braun implements one of the most detailed and representative approaches for predicting the impacts of simultaneous faults. When using the model, the user can be reasonably assured that mass and energy balances across the heat exchangers are maintained over the range of inputs. Additionally, differences between mass flow rates through the compressor and the expansion valves predicted by the model are driven to zero by the integrated cycle solver. It should also be noted that detailed charge inventory modeling based in part on empirical relationships tuned using experimental data is applied within the system model.

The detailed fault impact model developed by Cheung and Braun is not without at least one significant cost: the computational effort required for some combinations of faults and operating conditions can be significant. Even with the extreme speed of modern computer processors, simulating equipment performance using the detailed model can be time-consuming. In practice, the model often requires more than 30 seconds and multiple computer processor cores to simulate a single combination of inputs. When infrequent or one-off model evaluations are required, e.g. estimating steady-state fault impacts at a specific operating condition, the amount of computer time required is still insignificant to warrant optimization. However, if frequent or routine model function calls are required for an application, this time delay can be problematic. For example, if the average time requirement to predict equipment fault impacts is only 5 seconds, an 8760-hourly building simulation would require approximately 12 hours of computer time. As a result, this detailed model is not practical for inclusion within the simulation platform described in a companion paper by Hjortland and Braun that is used for assessing optimal and alternative service strategies (2018).

This paper describes a meta-modeling approach used to reduce the computational effort required to simulate DX equipment fault impacts without significantly sacrificing model accuracy. In the next section, artificial neural network models used to simulate equipment fault impacts are discussed. The model training and evaluation methodology is described for a RTU with a fixed orifice expansion device along with a discussion of some sample results. Following a description of the neural network meta-model, a description of the building model and fault evolution models used to characterize the operating cost impacts of different faults is described.

2. DESCRIPTION OF FAULT IMPACT META-MODEL

The detailed fault impact model developed by Cheung and Braun was used to generate outputs for training of a meta-model so that fault impact predictions could be generated at a much faster rate. This process, shown in Figure 1, was a supervised learning process where the underlying relationships between inputs and outputs of the original model were approximated. First, an extensive list of ambient conditions and fault levels were generated that spanned the range of operating conditions that were desired to be modeled. The ranges of ambient conditions and fault levels used to generate the data are described in Table 1. In all, 22,440 unique combinations of simulation parameters were simulated (with successful convergence criteria) using the detailed fault impact model. Next, these model inputs were fed to the detailed fault impact inverse model and one-by-one the outputs were collected. These input and output combinations were collated and consolidated into a training and validation data set.

Table 1. Range of detailed fault impact model simulation variables used to generate training and validation data sets for neural network meta-model.

Parameter	Minimum	Maximum	Increment
Outdoor Air Temperature	15.6 °C (60.0 °F)	48.9 °C (120.0 °F)	2.8 °C (5.0 °F)
Return Air Temperature	21.1 °C (70.0 °F)	29.4 °C (85.0 °F)	1.7 °C (3.0 °F)
Return Air Relative Humidity	30%	70%	5%
Refrigerant Charge Level[1]	60%	130%	5%
Condenser Fouling Level[2]	0%	50%	5%
Evaporator Fouling Level[3]	0%	50%	5%

[1] Charge level x_{chrg} defined based on rated charge level: $x_{chrg} = m_{actual} / m_{rated}$.

[2] Condenser fouling level defined as the relative reduction in condenser airflow rate compared to normal.

[3] Evaporator fouling level defined as the relative reduction in evaporator airflow rate compared to normal.

Next, the internal structure of an artificial neural network model was generated, and the internal weights were tuned using a supervisory learning setting. This means that a portion of the generated dataset was used to optimize the parameters of the neural network by minimizing the mean absolute error of the predicted outputs in comparison to the detailed model outputs. In order to do this in an efficient manner, highly optimized backpropagation algorithms and software packages were used (Chollet, 2015; Goodfellow, Bengio, & Courville, 2016). In an iterative manner, the resulting model was tested using the reserved validation portion of the generated data set to evaluate how well the model predicts data points not contained in the training data set. If undesirable or significant errors were observed in the resulting model, the model structure was modified, and the process was repeated.

A simplified schematic representation of the underlying neural network inputs, outputs, and inner layer nodes is shown in Figure 2. The inputs to the model are the ambient driving conditions of the DX system, including the outdoor air dry-bulb, return air dry-bulb, and return-air wet-bulb. The fault levels of the system were also given as inputs to the model. The outputs of the neural network meta-model were the refrigerant- and air-side state points that are determined by the original detailed fault impact model. These included suction pressure and enthalpy, liquid-line pressure and enthalpy, supply air temperature and humidity, etc. Connecting the inputs to the outputs were three layers containing so-called hidden nodes. These nodes are non-linear activation functions that are sequentially connected. The activation functions are typically sigmoidal or functions with an asymptote that are expressed in terms of a weighted combinations of inputs that are connected to it. These functions provided a highly non-linear behavior that can approximate complex interactions between inputs. The function weights used in each of these nodes were tuned during the model training process with backpropagation via stochastic gradient descent.

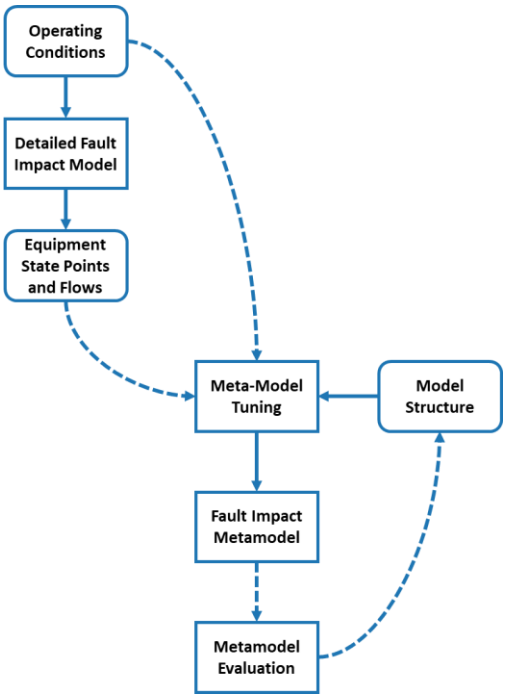

Figure 1. Overview of supervisory learning process used to develop fault impact meta-model using detailed fault impact model inputs and outputs.

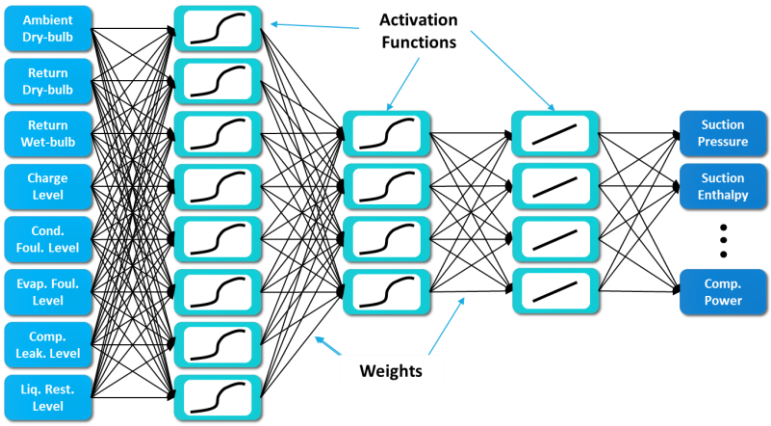

Figure 2. Simplified representation of the neural network meta-model used to approximate the detailed fault impact model developed by Cheung and Braun (2013a, 2013b).

To train the model while avoiding overfitting, the number of layers and hidden nodes were pruned using the combination of a training data set and a test data set. The activation functions selected for the model included hyperbolic tangent functions in the first two layers and a linear activation layer for the final layer. The training data set consisted of 17,952 combinations of inputs (80% of the total cases output from the original detailed model) and were randomly selected. The validation data set was made up of the remaining 4488 simulation outputs (20% of the total). The parameter tuning process of the model required approximately 90 minutes of computer time, utilizing two processor cores. Evaluating the resulting model required on the order of 10 μs for a combination of inputs – significantly faster than the original detailed model.

Using the tuned meta-model, refrigerant state points were predicted over the range of operating conditions and fault levels that were simulated using the detailed model implemented by Cheung and Braun (2013a, 2013b). These meta-model predictions were then compared with the detailed model outputs to evaluate the accuracy and reliability of using the meta-model. The suction pressure and enthalpy predicted by both models are compared for the entire dataset in Figure 3 for an RTU with fixed-orifice expansion valve (described in Table 2). In both cases, the agreement between the suction pressure and suction enthalpy were within 10% error for greater than 99.99% of the data set. Furthermore, the suction pressure predictions were within 5% error for greater than 90% of the data set; the suction enthalpy predictions were within 5% error for greater than 95% of the data set. It should also be noted that the range of suction pressures included in the data set was relatively large. The suction pressure ranged from 350 kPa (51 psia) to 1300 kPa (189 psia). At these pressures, the evaporator saturation temperature ranged from -23.1 °C (-9.5 °F) to 16.3 °C (61.4 °F), respectively. An actual RTU would more than likely be deactivated by low pressure cut-out safety or from a completely frosted evaporator coil. Because the detailed fault impact model did not model coil frosting or low pressure cutout safety measures, the accuracy of the meta-model at these conditions should be be treated with some skepticism since the underlying model has not be experimentally validated at these conditions.

Table 2. Description of detailed fault impact model system used to generate example results. System tested by Shen et al. (2009).

System Type	Packaged (RTU)
Rated Capacity	10.55 kW (3 ton)
Rated EER	10.6 BTU/W
Rated SEER	12.0 BTU/W
Refrigerant	R410A (3.24 kg)
Compressor	Fixed-Speed Scroll
Exp. Valve	Fixed Orifice
Condenser	Finned-Tube
Evaporator	Finned-Tube

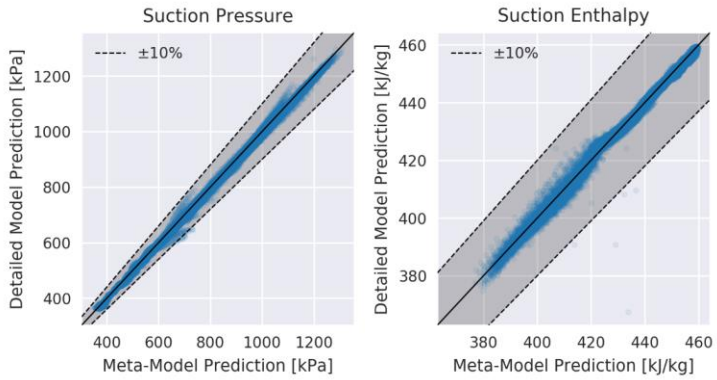

Figure 3. Overall comparison of suction pressure and enthalpy predictions from fault impact meta-model and detailed model for system with fixed orifice expansion valve.

As a further example of the model prediction accuracy, the liquid-line (condenser outlet) refrigerant pressure and enthalpy predicted by both models for the entire data set are compared in Figure 4. The predictions generated by each model for the liquid line pressure and enthalpy were within 5% for greater than 99.99% of the entire data set. Like the suction pressure results, the data set showed a relatively large range in liquid pressures: 1700 kPa (247 psia) to 4700 kPa (682 psia). Since the critical pressure of R410A is approximately 4578 kPa (664 psia), these data points should have been discarded from the data set. Moreover, these high pressures are surely outside the operating envelope of the compressor and the system would be disabled on high pressure cut-out safeties. These outputs should be discarded from the dataset for model evaluation since they would result in unreasonable equipment performance.

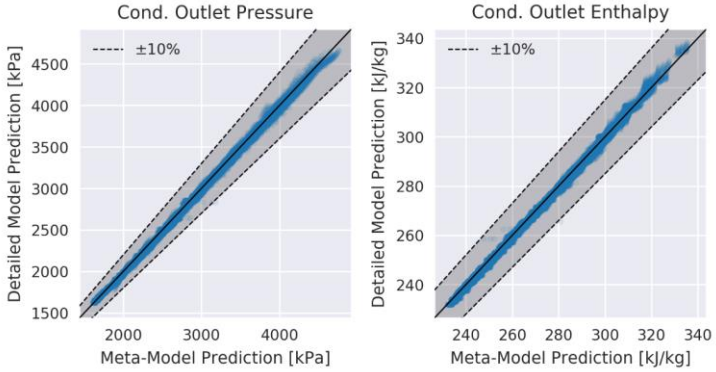

Figure 4. Overall comparison of liquid line (condenser outlet) pressure and enthalpy predictions from fault impact meta-model and detailed model for system with fixed orifice expansion valve.

Using the meta-model, the performance of the RTU was simulated at different ambient operating conditions and fault levels. The predicted total cooling capacity, coefficient of performance (*COP*), and sensible heat ratio (*SHR*) of the system at different ambient temperatures and fault levels has been plotted in comparison with the outputs of the original detailed model in Figure 5. Close agreement between the outputs of the meta-model and the detailed model were observed. More importantly, the meta-model outputs do not display signs of overfitting since the resulting outputs were mostly smooth, even where interpolation and extrapolation were required.

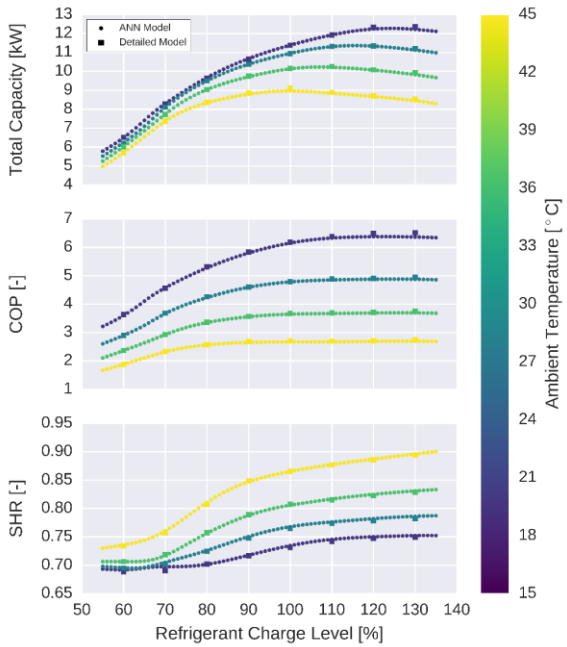

Figure 5. Modeled total cooling capacity, cycle *COP*, and *SHR* for RTU with fixed orifice expansion valve at different levels of refrigerant charge.

The meta-model was used to predict the performance of the RTU when the system is subjected to different levels of condenser fouling in Figure 6. Like the results shown for varying levels of refrigerant charge, good agreement was seen between the meta-model outputs and the original detailed model for condenser fouling faults at different ambient temperature conditions. The model also predicted more significant impacts on RTU efficiency than total cooling capacity as would be expected by condenser fouling faults.

A comparison of the predicted RTU performance with different combinations of ambient temperatures and evaporator fouling levels is shown in Figure 7. Again, good agreement between the two models is observed suggesting the neural network model approximates the physics of the detailed model well. Furthermore, it is important to note that both models predict relatively small impacts on cycle efficiency but large impacts on total cooling capacity and sensible heat ratio. This indicates both models produce outputs that are representative of actual evaporator fault impacts.

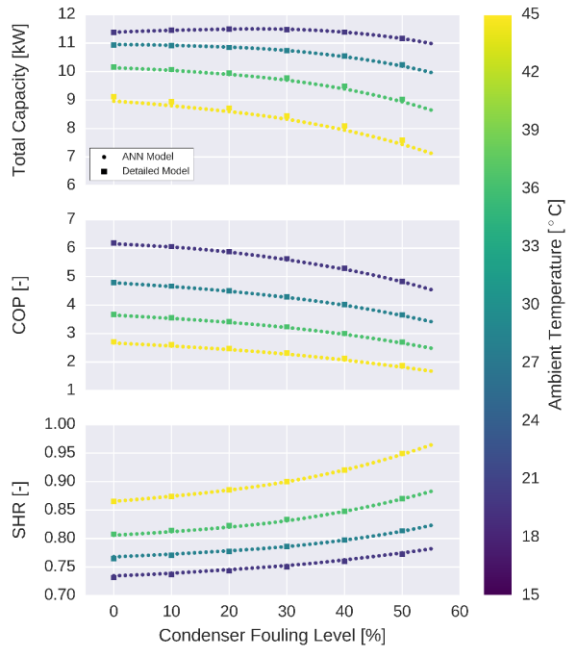

Figure 6. Comparison of modeled total cooling capacity, cycle *COP*, and *SHR* for RTU with fixed orifice expansion valve over a range of condenser fouling levels.

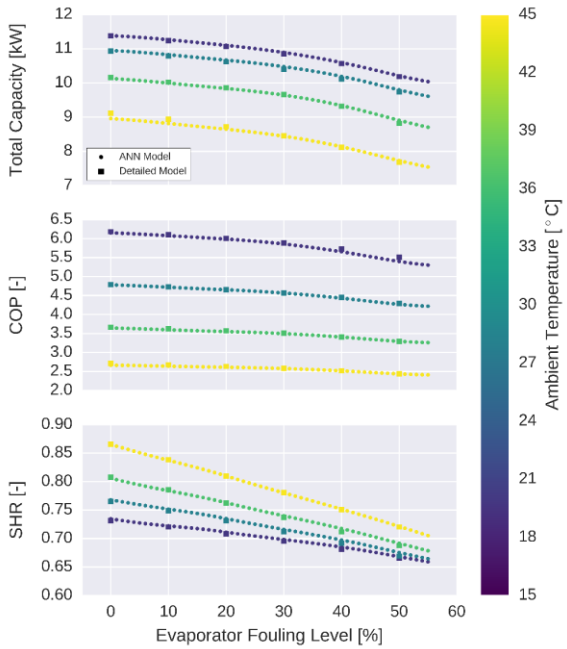

Figure 7. Comparison of modeled total cooling capacity, cycle COP, and SHR for RTU with fixed orifice expansion valve over a range of evaporator fouling levels.

3. BUILDING LOAD AND FAULT EVOLUTION MODELS

3.1 Building Load Model Description

The sensible and latent dynamics of a building served by a single RTU were simulated using simple, single-node models. The dynamics of the indoor dry bulb temperature were simulated using

$$C_s \frac{dT_{ID}}{dt} = \dot{Q}_{load,s} - \dot{Q}_{cool,s} \tag{1}$$

where T_{ID} is the indoor temperature, $\dot{Q}_{load,s}$ is the sensible heat gain in the building, $\dot{Q}_{cool,s}$ is the sensible cooling rate of the RTU, and C_s is the effective thermal capacitance of the building. The sensible heat gain of the building was based on an internally driven component $\dot{Q}_{int,s}$ and an externally driven component $\dot{Q}_{ext,s}$,

$$\begin{aligned} \dot{Q}_{load,s} &= \dot{Q}_{int,s} + \dot{Q}_{ext,s} \\ &= \dot{Q}_{int,s} + UA_s \cdot \left(T_{OD} - T_{ID}\right) \end{aligned} \tag{2}$$

where UA_s is the overall heat transfer conductance of the building and T_{OD} is the outdoor air dry bulb temperature. The sensible cooling rate of the system was simulated using the neural network meta-model discussed in Section 2. The required inputs of the meta-model were the outdoor dry bulb temperature, indoor dry bulb and wet bulb temperatures, and the fault levels of the equipment.

The internal gain and overall heat transfer conductance used in Equation (2) were determined for different climates using the commonly used balance point methodology based on equipment sensible capacity at the warmest condition (ASHRAE, 2017). The overall conductance was determined using

$$UA_s = \frac{\dot{Q}_{cool,s,design}}{1+f_{os}} \cdot \frac{1}{T_{OD,design} - T_{OD,balance}} \tag{3}$$

where $\dot{Q}_{cool,s,design}$ is the design point sensible cooling capacity of the equipment without faults, f_{os} is an equipment oversizing factor, $T_{OD,design}$ is the design point outdoor air dry bulb temperature, $T_{ID,design}$ is the design point indoor dry bulb temperature, and $T_{OD,balance}$ is the balance point outdoor dry bulb temperature when the building has no load. For all climates used for simulations, the design point temperature was chosen by finding the maximum outdoor air temperature using the weather data. The design point indoor dry bulb temperature set point was set to 75 °F. The balance point outdoor temperature was set to 65 °F for all climates. The internal sensible gain is given by

$$\dot{Q}_{int,s} = \frac{\dot{Q}_{cool,s,design}}{1+f_{os}} \cdot \frac{T_{ID,design} - T_{OD,balance}}{T_{OD,design} - T_{OD,balance}}. \tag{4}$$

An approximation of Equation (1) was implemented using a finite difference formula for the derivative term

$$T_{ID}(k+1) = T_{ID}(k) + \frac{\Delta t_{sim}}{C_s}\left[\dot{Q}_{int,s} + UA_s \cdot \left(T_{OD}(k) - T_{ID}(k)\right) - \dot{Q}_{cool,s}(k)\right] \tag{5}$$

where Δt_{sim} is the simulation time step size, $T_{ID}(k)$ is the indoor temperature at the k^{th} simulation step, and $T_{ID}(k+1)$ is the indoor temperature at the $(k+1)^{\text{th}}$ step. The simulation step size used for the model was 60 minutes.

The latent dynamics of the building were modeled using a single node dynamic energy balance,

$$C_l \frac{d\omega_{ID}}{dt} = \frac{1}{h_{fg,w}}\left[\dot{Q}_{load,l} - \dot{Q}_{cool,l}\right] \tag{6}$$

where ω_{ID} is the indoor air humidity ratio, $\dot{Q}_{load,l}$ is the latent heat gain in the building, $\dot{Q}_{cool,l}$ is the sensible cooling rate of the RTU, $h_{fg,w}$ is the heat of vaporization of water, and C_l is the effective thermal capacitance of the building. The latent heat gain of the building was based on an internally driven component $\dot{Q}_{int,l}$ and an externally driven component $\dot{Q}_{ext,l}$,

$$\begin{aligned} \dot{Q}_{load,l} &= \dot{Q}_{int,l} + \dot{Q}_{ext,l} \\ &= \dot{Q}_{int,s} + U_l \cdot \left(\omega_{OD} - \omega_{ID}\right) \end{aligned} \tag{7}$$

where U_l is the overall latent conductance of the building and ω_{OD} is the outdoor air humidity ratio. The conductance was determined using the equipment latent heat transfer rate at the design point condition,

$$U_l = \frac{\left(1 - SHR_{design}\right) \cdot \dot{Q}_{cool,t,design}}{1+f_{os}} \cdot \frac{1}{\omega_{OD,design} - \omega_{ID,balance}} \tag{8}$$

where $\dot{Q}_{cool,t,design}$ is the design point total cooling capacity of the equipment without faults, SHR_{design} is the design sensible heat ratio of the building, f_{os} is an equipment oversizing factor, $\omega_{OD,design}$ is the design point outdoor air humidity ratio, $\omega_{ID,design}$ is the design point indoor air humidity ratio, and $\omega_{OD,balance}$ is the balance point outdoor air humidity ratio when the building has no latent load. The design point indoor air humidity ratio was calculated using an indoor dry bulb temperature of 75 °F and relative humidity equal to 50%. For all climates used for simulations, the design point humidity ratio was chosen by finding the mean coincident wet bulb of the design outdoor air dry

bulb temperature. The balance point outdoor temperature was determined by finding the mean humidity ratio throughout the year using climate data. The internal latent gain is given by

$$\dot{Q}_{int,l} = \frac{\left(1 - SHR_{design}\right)\dot{Q}_{cool,t,design}}{1 + f_{os}} \cdot \frac{\omega_{ID,design} - \omega_{OD,balance}}{\omega_{OD,design} - \omega_{OD,balance}}. \quad (9)$$

An approximation of Equation (6) was implemented using a finite difference formula for the derivative term

$$\omega_{ID}\left(k+1\right) = \omega_{ID}\left(k\right) + \frac{\Delta t_{sim}}{C_l \cdot h_{fg,w}}\left[\dot{Q}_{int,l} + U_l \cdot \left(\omega_{OD}\left(k\right) - \omega_{ID}\left(k\right)\right) - \dot{Q}_{cool,l}\left(k\right)\right] \quad (10)$$

where $\omega_{ID}\left(k\right)$ is the indoor air humidity ratio at the k^{th} simulation step, and $\omega_{ID}\left(k+1\right)$ is the indoor air humidity ratio at the $\left(k+1\right)^{\text{th}}$ step.

In order to simulate equipment performance under realistic outdoor ambient conditions, Typical Meteorological Year (TMY) data was used (Wilcox & Marion, 2008). TMY data sets provide hourly ambient temperature, humidity, barometric pressure, irradiance, wind speed, and other weather data that represent a year of typical climatic conditions for a location (Wilcox & Marion, 2008). TMY data is commonly used by designers to model HVAC and energy conversion systems since the data provides reasonable driving conditions for assessing and comparing technologies. Three locations were selected for fault impact simulations: Atlanta, GA; Chicago, IL; and Miami, FL. These locations were selected because they have different amounts of cooling and heating requirements. Additionally, the average humidity through the year varies considerably from location to location. For each location, design conditions are summarized in Table 3 (ASHRAE, 2017). In order to size the building sensible cooling and heating load line in Equation (2), the maximum dry-bulb temperature for each location was determined. To determine the latent load line parameters in Equation (7), the coincident maximum humidity ratio during the hottest day of the year was determined.

Table 3. Building HVAC design conditions for selected locations used in fault impact simulation program (ASHRAE, 2017).

Location	HDB (99%)	CDB (1%)	MCWB (1%)	HDD	CDD
Atlanta, GA	-3.1 °C (26.4 °F)	33.1 °C (91.6 °F)	23.3 °C (73.9 °F)	1484 °C-day (2672 °F-day)	1052 °C-day (1894 °F-day)
Chicago, IL	-15.7 °C (3.7 °F)	31.5 °C (88.7 °F)	22.9 °C (73.2 °F)	3449 °C-day (6208 °F-day)	480 °C-day (864 °F-day)
Miami, FL	11.1 °C (52.0 °F)	32.7 °C (90.9 °F)	25.3 °C (77.5 °F)	70 °C-day (126 °F-day)	2521 °C-day (4538 °F-day)

HDB (99%) – 99th percentile design heating dry bulb temperature.
CDB (1%) – 1st percentile design cooling dry bulb temperature.
MCWB (1%) – 1st percentile design mean coincident wet bulb temperature.
HDD – Heating degree days calculated using 18.3 °C (65.0 °F) balance temperature.
CDD – Cooling degree days calculated using 18.3 °C (65.0 °F) balance temperature.

3.2 Fault Evolution Model Descriptions

Central to simulating the operating cost impacts of faults are models characterizing how faults may grow over time. The fault evolution models implemented in this work are simplistic in nature but provide reasonable estimations of real systems. Three faults are considered in this work: refrigerant charge leakage, condenser fouling, and evaporator fouling. A description of how each was modeled is discussed in this section.

The mass of refrigerant charge within the air conditioning system, m_{actual}, was modeled as a linear function of the time since service was last performed, $\Delta t_{service}$,

$$m_{actual} = \begin{cases} \left(1 - \frac{1}{2} \cdot \frac{\Delta t_{service}}{\Delta t_{chrg}}\right) \cdot m_{rated} & \text{for } 0 \le \Delta t_{service} \le \Delta t_{chrg} \\ \frac{1}{2} \cdot m_{rated} & \text{for } \Delta t_{service} > \Delta t_{chrg} \end{cases} \quad (11)$$

where m_{rated} is the rated amount of refrigerant in the system and Δt_{chrg} is the simulation time required for the system to leak 50% of the rated charge. In other words, Δt_{chrg} determines the refrigerant leakage rate from the system. Because the meta-model used to predict performance impacts of refrigerant charge faults cannot be verified below 50% charge levels, the minimum refrigerant charge level in the simulation was constrained to 50%. After the time since last service becomes greater than the leakage time parameter, the refrigerant charge level is fixed at 50%. While this limit was implemented, due to significant reductions in cooling capacity – comfort violations occurred before charge was reduced to 50% in the simulations performed. After refrigerant service is performed, the refrigerant charge in the system is returned to the rated level of charge.

Evaporator fouling was modeled by assuming dust and debris reduces evaporator air flow rate in the air conditioning system. As a function of the indoor fan run-time, Δt_{IDF}, the evaporator air flow rate, $\dot{V}_{ea,actual}$, was assumed to decrease linearly,

$$\dot{V}_{ea,actual} = \begin{cases} \left(1 - \frac{3}{5} \cdot \frac{\Delta t_{IDF}}{\Delta t_{ea,\,foul}}\right) \cdot \dot{V}_{ea,normal} & \text{for } 0 \le \Delta t_{IDF} \le \Delta t_{ea,\,foul} \\ \frac{2}{5} \cdot \dot{V}_{ea,normal} & \text{for } \Delta t_{IDF} > \Delta t_{ea,\,foul} \end{cases} \quad (12)$$

where $\Delta t_{ea,\,foul}$ is the indoor fan runtime required to cause a 60% reduction in air flow rate. When evaporator fouling service is performed in the simulation, the evaporator air flow rate is returned to the normal level. To prevent equipment model inaccuracies, the minimum air flow rate was restricted to 40% of the normal air flow rate. In the model, the indoor fan is assumed to run 100% of the time during occupied periods and when cooling is required during unoccupied periods.

In a similar manner, condenser fouling was modeled as a function of outdoor fan run-time, Δt_{ODF}, since the last service was performed. When condenser fouling occurs, the air flow through the condenser, $\dot{V}_{ca,actual}$ was reduced linearly according to,

$$\dot{V}_{ca,actual} = \begin{cases} \left(1 - \frac{3}{5} \cdot \frac{\Delta t_{ODF}}{\Delta t_{ca,\,foul}}\right) \cdot \dot{V}_{ca,normal} & \text{for } 0 \le \Delta t_{ODF} \le \Delta t_{ca,\,foul} \\ \frac{2}{5} \cdot \dot{V}_{ca,normal} & \text{for } \Delta t_{ODF} > \Delta t_{ca,\,foul} \end{cases} \quad (13)$$

where $\Delta t_{ca,\,foul}$ is the time required for the air flow through the condenser to reduce to 40% of the normal condenser air flow, $\dot{V}_{ca,normal}$. To prevent equipment model inaccuracies, the minimum condenser air flow rate was restricted to 40% of the normal air flow rate. Additionally, it was assumed that the outdoor fan operates only when the compressor operates, thus, the condenser fan run-time is equal to the run-time required for cooling.

In order to simulate comfort disturbances caused by high head pressure cut-out and low suction pressure cut-out safeties, the air conditioning system in the system was required to operate within an acceptable envelope. When the simulated discharge pressure was greater than 3890 kPa (550 psig), the cooling output of the system was assumed to be zero due to high-pressure limit cut-out. High pressure cut-outs most frequently were the result of system operating during warm ambient conditions with significant condenser fouling levels. When the suction pressure of the simulated system fell below 860 kPa (110 psig), no cooling was provided by the system since the low-pressure

limit cut-out was assumed to be activated. The safeties were automatically reset during the next simulation time step, provided the system pressures fell within the operating envelope.

3.3 Example Simulation Results

The equipment fault impact meta-model, building load model, and fault evolution models were integrated into a simulation tool and used to determine example simulation results for a building located in Miami, Florida over a three-year period. The equipment described by Table 2 was simulated in these examples. The building loads were scaled such that the sensible cooling capacity of the equipment on the warmest day of the year was 20% greater than the maximum load. Refrigerant charge leakage was modeled using Equation (11) with a leakage rate of 10% per year. The evaporator and condenser fouling rates were modeled using Equations (12) and (13) and with equivalent fouling rates of 5% per 5000 hours of fan run-time. For a system that is never serviced over the three-year simulation span, the trends in fault levels are shown in Figure 8. The ideal sensible cooling capacity for a system without faults, as well as the actual sensible cooling capacity is also shown in Figure 8. It is observed from the simulated results that the faults have a significant impact on cooling capacity over time when service is not performed. A comparison of the daily run-time requirement throughout the simulation is shown in Figure 9. Due to reduced system capacity, the system with faults must run longer to meet the cooling load within the building. The faults lead to reductions in COP and increases in energy consumption throughout the simulation, shown by Figure 9.

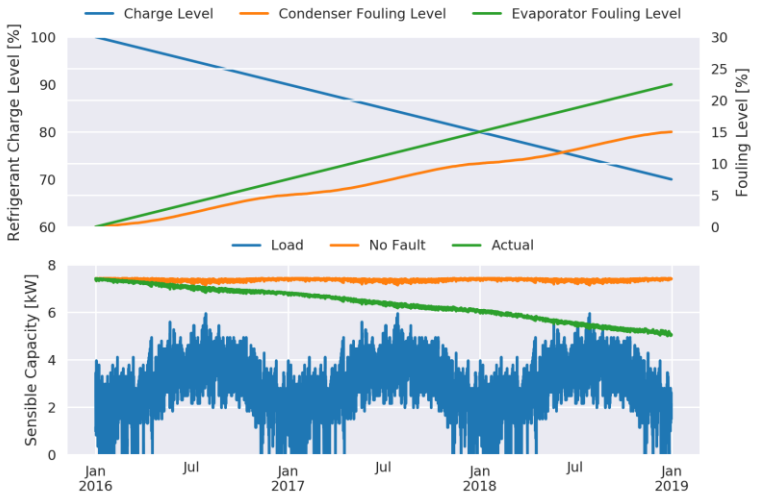

Figure 8. Simulated fault levels and comparison of sensible cooling capacity between system without faults and system with refrigerant charge leakage, condenser fouling, and evaporator fouling evolving over time.

For comparison, the same system was simulated again with maintenance performed annually. Each January, the maintenance was simulated by adjusting the refrigerant charge level and evaporator fouling level to their normal levels, shown in Figure 10. In comparison to the system that is not serviced, the cooling capacity impacts are noticeably less. Additionally, Figure 11 shows that the system operates with a higher average COP and consumes less energy relative to the system that is not serviced.

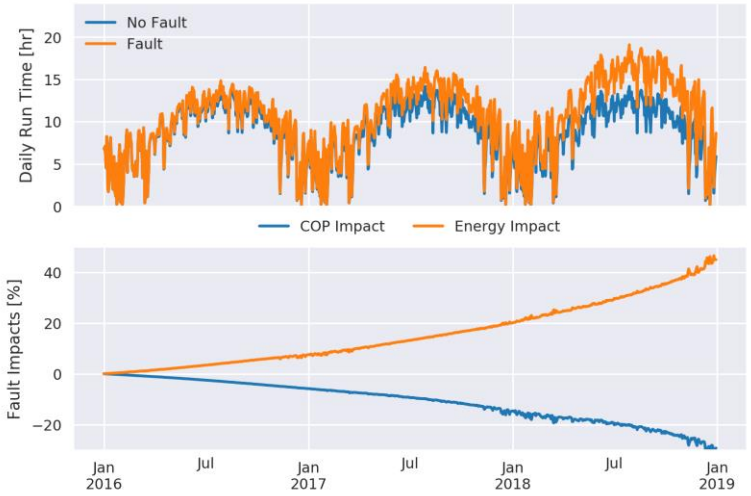

Figure 9. Comparison between system run-time for system with and without faults over three years. Also show is the relative fault impacts on COP and energy consumption.

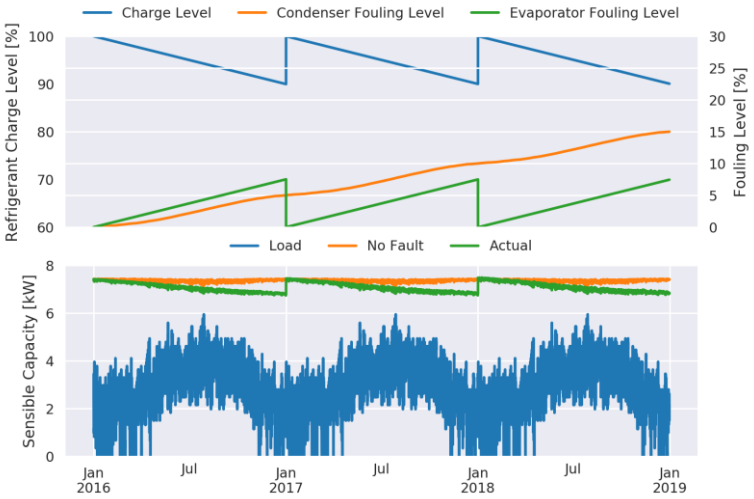

Figure 10. Comparison between sensible cooling capacity for system without faults and system that receives refrigerant charge and evaporator fouling service annually.

4. CONCLUSIONS

A neural network meta-model has been shown to generate accurate results that approximate the outputs of a detailed grey box fault impact model developed and validated by Cheung and Braun (2013a, 2013b). The outputs of this meta-model overcome one of the major limitations of the original model – the solution time required. One issue remains with both models – the amount of experimental data required to accurately tune the model is relatively high and the resulting model is not generalizable to all systems. While it is unlikely that manufacturers would be able to develop sufficient testing resources for developing neural network models of equipment performance to predict the impacts caused by different faults, it should be reiterated that these models are useful for the present work in evaluating alternative service policies (see Hjortland and Braun, 2018). In an ideal setting, it would be possible to use detailed physical models for analyzing the performance of fault impact models and performing parametric studies of different optimal service scheduling strategies. However, with the current performance limits of computing systems, it would not be possible to adequately analyze all the possible combinations of faults in a reasonable amount of time. These limitations could be overcome using the neural network models described in this

work. Using the extensive datasets collected from previous researchers, the detailed fault impact models developed by Cheung and Braun were possible (2013a, 2013b). Rather than applying this model directly, the neural network models were designed to approximate the relationship between the inputs and outputs of the detailed inverse models with much greater speed. The methodology could be applied to any detailed physical model to approximate outputs using much less computing resources. These models can then be used to develop less complex models that manufacturers are able to implement.

In conclusion, the neural network models developed are not intended to be viewed as a solution to be used to estimate fault impacts in practice. Rather, they will be used to assess simplified models and strategies for implementing condition-based maintenance. An example simplified building load model and fault evolution models have been described in this work. In a companion work, Hjortland and Braun use the models developed here to compare different maintenance strategies for commercial buildings (2018).

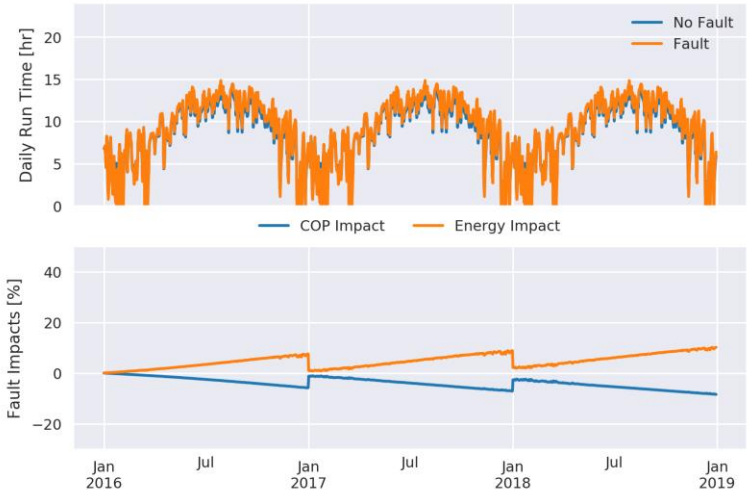

Figure 11. When refrigerant charge and evaporator fouling service is performed annually, the run-time impacts of faults becomes relatively small. The relative impacts on COP and energy consumption is reduced as well.

REFERENCES

ASHRAE. (2017). *Handbook of Fundamentals*. Atlanta, GA: American Society of Heating, Refrigeration, and Air-Conditioning Engineers.

Cheung, H., & Braun, J. E. (2013a). Simulation of Fault Impacts for Vapor Compression Systems by Inverse Modeling. Part I: Component Modeling and Validation. *HVAC&R Research, 19*(7), 26.

Cheung, H., & Braun, J. E. (2013b). Simulation of Fault Impacts for Vapor Compression Systems by Inverse Modeling. Part II: System Modeling and Validation. *HVAC&R Research, 19*(7), 15.

Chollet, F. (2015). Keras: Github. Retrieved from https://github.com/fchollet/keras

Goodfellow, I., Bengio, Y., & Courville, A. (2016). *Deep Learning*. Cambridge, MA: MIT Press.

Hjortland, A. L., & Braun, J. E. (2018). *Simulating and Comparing Maintenance Strategies for Rooftop Units with Multiple Faults*. Paper presented at the International Refrigeration and Air Conditioning Conference, West Lafayette, Indiana.

Shen, B., Braun, J. E., & Groll, E. A. (2009). Improved methodologies for simulating unitary air conditioners at off-design conditions. *International Journal of Refrigeration, 32*(7), 1837-1849. doi:10.1016/j.ijrefrig.2009.06.009

Wilcox, S., & Marion, W. (2008). *Users Manual for TMY3 Data Sets*. Retrieved from Golden, CO: